Infrared micro-emitters made by pulsed laser deposition lift-off-based processing

A. Gassenq, Y. Guyot, E. Cleyet-Merle, Sébastien Cueff, Hai Son Nguyen, A. Pereira

Infrared micro-emitters made by pulsed laser deposition lift-off based processing

A. Gassenq,[1*] Y. Guyot,[1] E. Cleyet-Merle,[1] S. Cueff,[2] H-S Nguyen,[2] A. Pereira,[1]

[1] *Université de Lyon, Institut Lumière Matière, UCBL, CNRS, UMR5306, F-69622, LYON, France.*

[2] *Institut des Nanotechnologies de Lyon, UMR 5270, CNRS, ECL, INSA, UCBL, F-69134, LYON, France*

Abstract

Micro-structuration of rare earth doped materials by lift-off processing of pulsed laser deposited layers are promising in integrated optics since they do not require complex processing. However, they are so far limited to Y_2O_3 host and have never been reported for infrared emission, which have many applications in telecommunication, sensing and so on. In this work, we have studied micro-devices made by pulsed laser deposition combined to lift-off processing on Si, with Er doped materials that have infrared emission at 1.54µm wavelength, corresponding to the $^4I_{1\ 3/2} \rightarrow {}^4I_{1\ 5/2}$ Er^{3+} transition. Two host materials have been compared: Al_2O_3 commonly used in integrated optics and Y_2O_3, which is a well-known crystalline host for rare earth doping. For both materials, micro-photoluminescence measurements combined with X-ray diffraction showed efficient incorporation of Er^{3+} ions into the host matrix, associated with strong emission when the matrix is amorphous for Al_2O_3 or crystalline for Y_2O_3. Thus, this work extends the pulsed laser deposition lift-off processing to other materials and wavelength range, which opens the way of easy realization of infrared micro-emitter for photonics applications.

* *Corresponding author: alban.gassenq@univ-lyon1.fr*

1. Introduction

Over the last decades, Silicon (Si) photonics has shown great interest in optics and optoelectronic applications. However, Si is not suitable for light emission due to its indirect band gap, therefore integrating active materials like Rare Earth (RE) elements on Si is of great interest [1–5]. RE emitters have been studied for a while in optics [6,7] and are now emerging as very interesting platform for quantum photonics [8,9]. Indeed, the lanthanide high coherences [10] allowing to realize many quantum functions such as single photon sources [11], memories [12–14], microwave transductors [15] and so on. For their patterning, bonding [4], masked deposition [1,16], additional layer [17], or etching [18,19] technics are commonly used. Such processing steps are costly and/or potentially detrimental for practical applications. Recently, we have shown that Y_2O_3:Eu^{3+} rare earth micro-emitters deposited by Pulsed Laser Deposition (PLD) and lift-off processing are promising for the integration of active micro-devices such as rare earth emitters on Si substrate in the visible wavelength range [20]. Indeed, since PLD deposition can provide high quality films at low temperature deposition due to the high kinetic energy of the atoms during the deposition [21], it is a compatible technique with the lift-off processing [22] to obtain micro-emitters on top of silicon without etching [20]. However, such demonstration was limited to visible wavelength emission related to Eu^{3+} doped Y_2O_3. Since Er^{3+} ions have a strong emission at ~1.54 μm due to the $^4I_{1\ 3/2} \rightarrow {}^4I_{1\ 5/2}$ transition widely studied in integrated optics [1–3,23–26], its makes it a suitable RE element for Infra-Red (IR) emission by down conversion. In the literature, Al_2O_3 [2,18,24,25,27] and Y_2O_3 [28–31] materials are used for Er^{3+} ions incorporation in photonics due to their compatibility with RE elements and their wide transparency from the ultra violet to IR range. They present different advantages and drawbacks. Al_2O_3 is a cheap and available material which is CMOS compatible for industrial applications [27,32,33], it presents low optical losses [33] but it is mainly used in amorphous configuration leading to a broad spectral emission [2,18,24,25]. Y_2O_3 is a suitable material for Er^{3+} ions incorporation in crystalline host matrix because Er and Y have similar atomic radius [28–31,34]. In that case, narrower emission is obtained compared to amorphous material but low propagation losses were reported only for high temperature deposition [34]. In this work, we have investigated IR Er-doped microstructures made by PLD and lift-off processing. We have first investigated PLD targets with both Al_2O_3 and Y_2O_3 host matrix for different doping levels. We have then deposited and patterned Er^{3+} doped Y_2O_3 and Al_2O_3 layers on Si, and characterized them by Energy-Dispersive X-ray (EDX), X-Ray Diffraction (XRD) and micro Photo-Luminescence (PL). We show that strong IR emission at the micro scale can be obtained with controlled spectra shape due to the intrinsic properties of the material host (i.e amorphous or crystalline). Therefore, our work highlight the PLD lift-off based processing as very interesting method to fabricate IR micro-emitter for photonics applications.

2. Target fabrication

We have first studied PLD targets. In PLD, an intense pulsed laser beam is focused through an optical window on a target under vacuum. If the target absorbs enough energy which depends of the used material [35,36] and morphology, the laser-material interaction leads to the formation of a plasma leading to the deposition of ablated species on the substrate facing the target. PLD targets are thus fundamental for the quality of the deposition [21]. In that respect, two kinds of PLD targets: $Al_2O_3:Er^{3+}$ and $Y_2O_3:Er^{3+}$, have been synthesized by solid-state reaction. The targets were fabricated by grinding and mixing powders of 99.99% purity (Er_2O_3, Al_2O_3 and Y_2O_3 from SIGMA ALDRICH). Powders were first mixed together and compressed under 7000 kg for 20 min for 2 cm diameter targets (~22 MPa). They were then annealed for 8 h-1400 °C with a 5 °C/min ramp for the temperature increase. Afterward, they were grinded, compressed the same way again, and annealed a second time with the same parameters. Doping concentration were calculated with the mass ratio of the mixed powders. Figure 1 a and b present the measured X-ray diffraction of $Al_2O_3:Er^{3+}$ (Figure 1-a) and $Y_2O_3:Er^{3+}$ (Figure 1-b) targets for several Er concentration. 2θ scan were performed with an AERIS PAN-analytic instrument from 20 to 55° using Cu-Kα radiation at λ = 1.540598Å, with a step size of 0.0109° and a counting time of 40s. All the diffracted peaks have been identified using Crystallography Open Database (COD) database and VESTA software. For $Al_2O_3:Er^{3+}$ (Figure 1-a), we found that α-Al_2O_3 is the main phase of the target (COD Al_2O_3-9009671). However, due to the Er insertion, $Al_5Er_3O_2$, $AlErO_3$ and Er_2O_3 compound were also identified (COD $Al_5Er_3O_2$-4312131, $AlErO_3$-2310399 and Er_2O_3-1534952, respectively). Furthermore, we notice that peaks corresponding to $Al_5Er_3O_2$ increase with Er concentration (see the peaks "*" at around 33° in the Figure 1-a, for instance) while other peaks have similar intensity. Therefore, the doping incorporation is not efficient because it creates AlErO alloys instead of replacing Al by Er in the Al_2O_3 host matrix since the crystal radius of Er is very different than Al (1.03 Å versus 0.67 Å for the VI coordination [37]). For $Y_2O_3:Er^{3+}$ (Figure 1-b), XRD patterns show that only Y_2O_3 and Er_2O_3 peaks are detected (COD Er_2O_3-1534952, Y_2O_3-1541743, respectively) at the same angles because Er and Y have similar atomic radius [37].

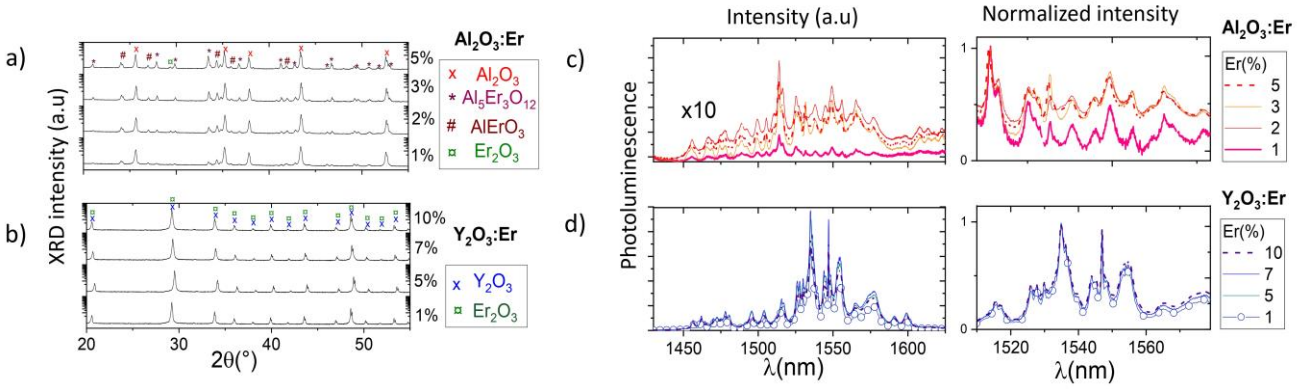

FIG. 1: PLD targets study with XRD measured pattern for (a) Al_2O_3:Er with 1 to 5 % doping concentration and (b) Y_2O_3:Er with 1 to 10 % doping concentration; associated PL measurements for (c) Al_2O_3:Er and (d) Y_2O_3:Er targets.

Figure 1-c and d presents PL measurements of the fabricated targets previously studied by XRD (Figure 1 a and b). Emission spectra measurements were recorded under 405 nm Continuous Wave (CW) laser diode excitation up to 200 mW, with a Andor Shamrock 500i mono-chromator and a Andor InGaAs detector, with a 300 lines/mm grating blazed at 1 µm. For $Y_2O_3:Er^{3+}$, we got an IR emission corresponding to the expected $^4I_{1\ 3/2} \rightarrow {}^4I_{1\ 5/2}$ transition of Er^{3+} ion [38] in good agreement with the literature for Y_2O_3 host matrix [30,31,39]. Furthermore, by comparing the normalized intensity, the shape of the spectra is relatively constant confirming the good Er incorporation. For $AlO_3:Er^{3+}$, intensity is lower. Emission spectra are obviously completely different than the usual Er doped amorphous Al_2O_3 [24,25,40–43]. For low Er content, many peaks are detected, potentially related to Al_2O_3:Er [39] and $Al_5Er_3O_{12}$ [44,45]. For high Er content, the normalized signal increases at higher wavelength nm, which could be attributed to $AlErO_3$ [46] and Er_2O_3 [47] alloys in good agreement with the XRD measurement (Figure 1-a). Figure 2-a presents the diffracted peaks Full Width at Half Maximum (FWHM) extracted from the Figure 1-a and 1-b, for Er doped Y_2O_3 and Al_2O_3 targets as a function of the Er content along the (102) direction at ~26° and (222) direction at ~29°, respectively. Similar trends are observed for other peaks. For Y_2O_3, the FWHM increases with Er content which can be related to a strain increase due to a good Er incorporation in the crystal. For Al_2O_3, the FWHM decreases which can be attributed to bigger Al_2O_3 grain sizes (at around 78 nm grain size following Scherrer equation) due to the difficulty of incorporating Er in this host matrix. Figure 2-b shows the difference between the integrated PL signal as function of the doping concentration for both materials. First, we clearly see that PL intensity increases with the doping concentration up to a relatively constant value after 2 %, we will thus choose the 5 % targets for both materials for the following of this study. Secondly, since the scale is not linear for a better viewing, integrated signal is 15 times higher for Y_2O_3 confirming the bad Er incorporation in Al_2O_3 host

matrix. Indeed, as indicated above the difference between the Er and Y are small (crystal radius of 1.03 Å and 1.04 Å with VI coordination) while for Al is 0.67 Å [37]. Furthermore, Y_2O_3 and Er_2O_3 also share the same cubic crystalline structure. Therefore, Y_2O_3 appears here as a very compatible crystalline host for Er^{3+} incorporation while Al_2O_3 layers is more suitable as amorphous host [2,18,24,25,40–43].

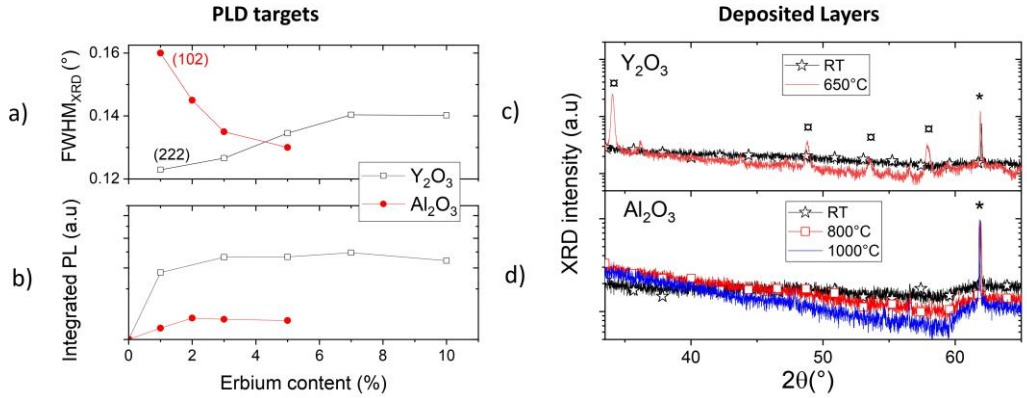

FIG. 2: comparison between Er doped Al_2O_3 and Y_2O_3 PLD target with (a) FWHM XRD peaks and (b) integrated PL signal as a function of Er content; XRD pattern for c) Y_2O_3:Er^{3+} and d) Al_2O_3:Er^{3+} layers deposited on Si substrate before and after annealing.

3. Layers deposition and microstructures fabrication

We have then deposited Er doped Al_2O_3 and Y_2O_3 layers on undoped (100) Si substrate with such targets. 500 nm thick Y_2O_3:Er^{3+} and Al_2O_3:Er^{3+} layers were deposited with 5 % Er on Si substrate with a KrF excimer laser (λ=248 nm, t=17 ns, Coherent Compex Pro) operating at 5 Hz. The laser beam was focused on the target over 2 mm^2, and the laser energy and the target-substrate distance were kept constant at 73 mJ (3.65 J/cm^2) and 6 cm, respectively. The films were grown with substrate rotation at room temperature in an oxygen-gas atmosphere (10^{-3} mbar) to obtain dense and stoichiometric Y_2O_3 or Al_2O_3. Such parameters have been fixed in order to have homogeneous deposition rate in the range of 3.5 nm/min [17,48,49]. After the deposition, samples were annealed for 24 h at different temperature in order activate the doping and to improve the film quality. Figures 2 c and d present the effect of the annealing for both layers on XRD pattern. The same XRD equipment and parameters presented for the Figure 1 a and b were used. As already reported for Y_2O_3:Eu^{3+} layers [20], annealing induces the crystallization of the Y_2O_3:Er^{3+} layer with the same cubic phase as the target (COD Y_2O_3-1541743 and indicated by the "¤" symbols in the Figure 3-a). We note that the "*" peaks correspond to the Si substrate [50] which is detected also before the annealing. For Al_2O_3, no crystallization occurs even at 1000 °C since higher temperature are needed to reach a good α crystallization [51].

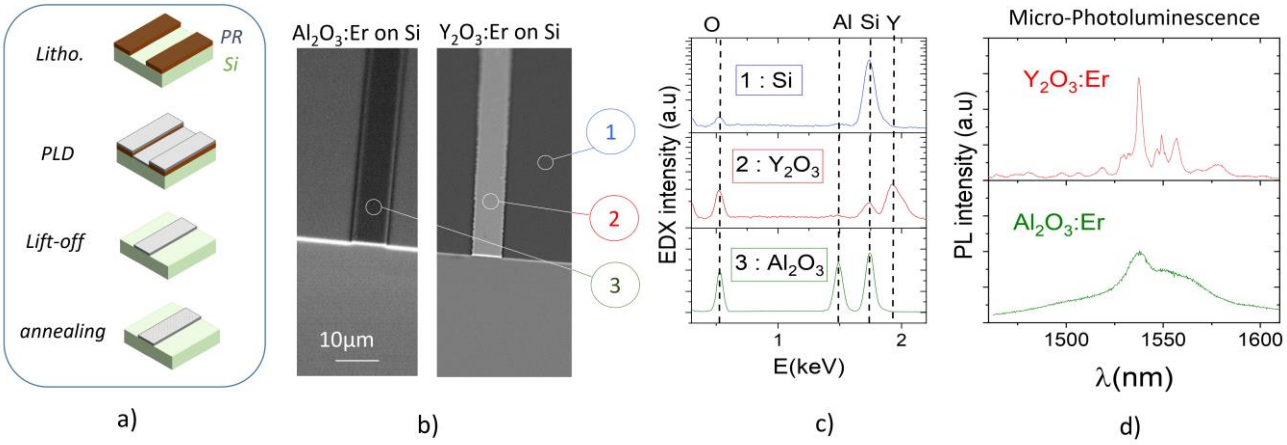

FIG. 3. a) Process flow for the IR micro-emitters fabrication using lithography, PLD deposition, lift-off and annealing; b) SEM 45° tilted image for doped oxide microstructure on Si and c) associated EDX measurements; d) micro-PL on $Y_2O_3:Er^{3+}$ and $Al_2O_3:Er^{3+}$.

Finally, we have fabricated Al_2O_3 and Y_2O_3 Er doped microstructures. The process flow is presented in Figure 3-a. 1.8 µm thick AZ5214E negative Photo-Resist was coated on silicon substrate. Insolations have been done using laser lithography with 8 µm width strip. We have then deposited 500 nm thick $Y_2O_3:Er^{3+}$ or $Al_2O_3:Er^{3+}$ layers by PLD with the same parameters presented above followed by the lift-off performed in ultrasonic wet bench for 30 s. After the patterning, the sample has been annealed for 24h at 650 °C for Y_2O_3 and 800 °C for Al_2O_3. The Figure 3 b and c presents Scanning Electron Microscopy (SEM) imaging and the associated EDX spectroscopy measurements of a fabricated micro-strips on Si. Such measurements were performed with a PHENOM G-Pro SEM at 15 keV. Two regions were compared (i.e out and on the micro-devices) for both $Al_2O_3:Er^{3+}$ and $Y_2O_3:Er^{3+}$ microstructures. The region 1 was measured out of the rare earth doped layers while the regions 2 and 3 were recorded on the $Y_2O_3:Er^{3+}$ and $Al_2O_3:Er^{3+}$ strips, respectively. According to EDX measurements (Figure 3-c), Y and Al atoms are detected only on the strip regions, indicating that no PLD material is out of the strip, which confirm the accuracy of the processing. Figure 3-d presents the micro-PL measurements performed with 532 nm wavelength CW laser focused over few µm² on the doped layers. Light was collected through a x50 objective and sent to a grating spectrometer with an IR InGaAs camera used as output detector. First of all, similar intensities are detected for both materials, which highlight the high quality of the micro-devices after annealing. Secondly, for Y_2O_3, the same transitions are found compared to the PLD target (Figure 1-d) in good agreement with the literature for $Y_2O_3:Er^{3+}$ [30,31], since the deposited layer is polycrystalline like measured by the XRD (Figure 2-c). For Al_2O_3, after annealing, emission is broader in good agreement with the literature [24,25,40–43] since the

host matrix is amorphous as indicated by the XRD measurements (Figure 2-d). Therefore, we have shown here that our liftoff based PLD technics can also provide high quality IR luminescent microstructures (in good agreement with other technics [30,31,40–42]) but without etching. Furthermore, we also highlight here the advantages and drawbacks of both Y_2O_3 and Al_2O_3 host materials for Er incorporation. Indeed, since we have use PLD deposition at room temperature we typically obtain amorphous layers after deposition [52]. As indicated by the XRD measurement, after annealing Y_2O_3 become crystalline [53] but Al_2O_3 stays amorphous at such temperature range [51,54]. Er emission is thus narrower in Y_2O_3, which can be interesting for spectroscopic application, while Er emission is larger in Al_2O_3, but the material host stay amorphous which can be relevant for low losses light propagation [27,33].

4. Conclusion

In Summary, we have investigated IR Er^{3+} doped microstructures made by PLD and lift-off processing. We have first investigated PLD targets with different doping levels in both Al_2O_3 and Y_2O_3 host matrix. XRD pattern shows that Er^{3+} ions doping incorporation is easier in Y_2O_3 matrix given one order of magnitude higher PL signal compared to Al_2O_3. We have then deposited Er-doped Y_2O_3 and Al_2O_3 layers. After annealing, XRD measurements show that only Y_2O_3 layers are crystalline while Al_2O_3 doped layers stay amorphous. Finally, Er-doped Y_2O_3 and Al_2O_3 micro-strips were fabricated by PLD lift-off processing. After annealing, both layers show strong IR emission at around 1.54 µm wavelength. Broader emission is obtained for Al_2O_3 host matrix since it is an amorphous material, while Y_2O_3 presents narrower emission due to a crystalline environment. We highlight thus the advantages and drawback of both material hosts. Therefore, this work extends the PLD liftoff-based processing method to other materials and wavelength range applications confirming that such processing method is a very interesting way to fabricate micro-emitter without etching. It opens perspective to the easy realization of IR microstructures for integrated optics. This work could be continued by the careful investigation of the microstructures morphologies as a function of the processing and deposition parameters.

Acknowledgements

The authors would like to thank the NanoLyon platform for the cleanroom facilities. Salahedine Toubi, Ylyes Betka and the Institute Light Matter for funding.

Declarations

Conflict of interest: The authors declare that they have no conflict of interest.

Ethics approval and consent to participate: All authors approved the submission.

References

1. N. Li, M. Xin, Z. Su, E. S. Magden, N. Singh, J. Notaros, E. Timurdogan, P. Purnawirman, J. D. B. Bradley, and M. R. Watts, Sci. Rep. **10**, 1 (2020).

2. J. Rönn, W. Zhang, A. Autere, X. Leroux, L. Pakarinen, C. Alonso-Ramos, A. Säynätjoki, H. Lipsanen, L. Vivien, E. Cassan, and Z. Sun, Nat. Commun. **10**, 1 (2019).

3. P. Xing, G. F. R. Chen, X. Zhao, D. K. T. Ng, M. C. Tan, and D. T. H. Tan, Sci. Rep. **7**, 1 (2017).

4. X. Jiang, D. Pak, A. Nandi, Y. Xuan, and M. Hosseini, Appl. Phys. Lett. **115**, 1104 (2019).

5. N. Li, E. S. Magden, Z. Su, N. Singh, A. Ruocco, M. Xin, M. Byrd, P. T. Callahan, J. D. B. Bradley, D. Vermeulen, and M. R. Watts, Opt. Express **26**, 4560 (2018).

6. D. L. Chubb, A. T. Pal, M. O. Patton, and P. P. Jenkins, J. Eur. Ceram. Soc. **19**, 2551 (1999).

7. J. H. Park and A. J. Steckl, J. Appl. Phys. **98**, 2003 (2005).

8. T. Zhong and P. Goldner, Nanophotonics **8**, 2003 (2019).

9. P. Stevenson, C. M. Phenicie, I. Gray, S. P. Horvath, S. Welinski, A. M. Ferrenti, A. Ferrier, P. Goldner, S. Das, R. Ramesh, R. J. Cava, N. P. de Leon, and J. D. Thompson, Phys. Rev. B **105**, (2022).

10. P. Siyushev, K. Xia, R. Reuter, M. Jamali, N. Zhao, N. Yang, C. Duan, N. Kukharchyk, A. D. Wieck, R. Kolesov, and J. Wrachtrup, Nat. Commun. **5**, 1 (2014).

11. 6 Kangwei Xia 1, 2 Fiammetta Sardi 1 7 † Colin Sauerzapf 1 Thomas Kornher, H.-W.

Becker, Z. Kis, L. Kovacs, D. Dertli, J. Foglszinger, R. Kolesov, and J. Wrachtrup, Optica **9**, (2022).

12. M. Raha, S. Chen, C. M. Phenicie, S. Ourari, A. M. Dibos, and J. D. Thompson, Nat. Commun. **11**, 1 (2020).

13. J. M. Kindem, A. Ruskuc, J. G. Bartholomew, J. Rochman, Y. Q. Huan, and A. Faraon, Nature **580**, 201 (2020).

14. A. Ruskuc, C. J. Wu, J. Rochman, J. Choi, and A. Faraon, Nature **602**, 408 (2022).

15. J. G. Bartholomew, J. Rochman, T. Xie, J. M. Kindem, A. Ruskuc, I. Craiciu, M. Lei, and A. Faraon, Nat. Commun. **11**, (2020).

16. R. W. Eason, T. C. May-Smith, C. Grivas, M. S. B. Darby, D. P. Shepherd, and R. Gazia, Appl. Surf. Sci. **255**, 5199 (2009).

17. N. V. Hoang, A. Pereira, H. S. Nguyen, E. Drouard, B. Moine, T. Deschamps, R. Orobtchouk, A. Pillonnet, and C. Seassal, ACS Photonics **4**, 1705 (2017).

18. L. Agazzi, J. D. B. Bradley, M. Dijkstra, F. Ay, G. Roelkens, R. Baets, K. Wörhoff, and M. Pollnau, Opt. Express **18**, 27703 (2010).

19. S. Dutta, E. A. Goldschmidt, S. Barik, U. Saha, and E. Waks, Nano Lett. **20**, 741 (2020).

20. A. Gassenq, E. Cleyet-Merle, H. Sahib, B. Baguenard, A. Belarouci, R. Orobtchouk, F. Lerouge, S. Guy, and A. Pereira, Opt. Express **29**, 7321 (2021).

21. H. Fujioka, Handb. Cryst. Growth Thin Film. Ep. **8**, 365 (2015).

22. J. Y. min Lee, M. M. Dange, and K. Sooriakumar, Microelectron. Eng. **18**, 215 (1992).

23. J. D. B. Bradley and M. Pollnau, Laser Photonics Rev. **5**, 368 (2011).

24. G. Dingemans, A. Clark, J. A. Van Delft, M. C. M. Van De Sanden, and W. M. M. Kessels, J. Appl. Phys. **109**, 113107 (2011).

25. M. Pollnau and J. D. B. Bradley, Opt. Express **26**, 24164 (2018).

26. A. Ruiz-Caridad, S. Collin, C. Alonso-Ramos, G. Agnus, S. Guerber, C. Baudot, F. Boeuf, S. Monfray, S. Cremer, V. Vakarin, E. Cassan, G. Marcaud, D. Marris-Morini, P. Lecoeur, L. Vivien, J. M. Ramirez, J. Zhang, E. Duran-Valdeiglesias, C. Lafforge, L. Largeau, T. Maroutian, and S. Matzen, IEEE J. Quantum Electron. **56**, 1 (2020).

27. W. A. P. M. Hendriks, L. Chang, C. I. van Emmerik, J. Mu, M. de Goede, M. Dijkstra, and S. M. Garcia-Blanco, Adv. Phys. X **6**, 1 (2021).

28. A. Peeva, A. O. Dikovska, P. A. Atanasov, M. J. de Castro, and W. Skorupa, Appl. Surf. Sci. **253**, 8165 (2007).

29. M. A. Gomes, S. M. V Novais, S. Macedo, A. C. Brand, J. F. M. Avila, J. J. R. Jr, and M. A. R. C. Alencar, J. Alloy. Compd. J. **731**, 478 (2018).

30. M. J. Lo Faro, A. A. Leonardi, F. Priolo, B. Fazio, M. Miritello, and A. Irrera, Sci. Rep. **10**, 1 (2020).

31. and P. B. A. N. Georgobiani, A. N. Gruzintsev, C. Barthou, Inorg. Mater. **40**, 963 (2004).

32. G. N. West, W. Loh, D. Kharas, C. Sorace-Agaskar, K. K. Mehta, J. Sage, J. Chiaverini, and R. J. Ram, APL Photonics 026101 (2019).

33. D. J. Blumenthal, APL Photonics **5**, 020903 (2020).

34. M. B. Korzenski, P. Lecoeur, B. Mercey, P. Camy, and J. L. Doualan, Appl. Phys. Lett. **78**, 1210 (2001).

35. L. Saravanan and T. Senthilvelan, J. Optoelectron. Photonics **5**, 14 (2015).

36. V. H. Mudavakkat, V. V. Atuchin, V. N. Kruchinin, A. Kayani, and C. V. Ramana, Opt. Mater. (Amst). **34**, 893 (2012).

37. A. S. Group, (2022).

38. D. G. O'Shea, J. M. Ward, B. J. Shortt, and S. Nic Chormaic, IEEE Photonics Technol. Lett. **19**, 1720 (2007).

39. T. Sanamyan, R. Pavlacka, G. Gilde, and M. Dubinskii, Opt. Mater. (Amst). **35**, 821 (2013).

40. J. C. Barbour, B. G. Potter, D. M. Follstaedt, J. A. Knapp, and M. B. Sinclair, MRS Online Proc. Libr. **438**, 465 (2017).

41. G. N. van den Hoven, A. Polman, E. Alves, M. F. da Silva, A. A. Melo, and J. C. Soares, J. Mater. Res. **12**, 1401 (1997).

42. J. Rönn, L. Karvonen, A. Pyymäki-Perros, N. Peyghambarian, H. Lipsanen, A. Säynätjoki, and Z. Sun, Proc. SPIE - Integr. Opt. Devices, Mater. Technol. **9750**, P1 (2016).

43. C. Fan, J. Wang, N. Tang, H. Xu, G. Wei, and H. Xu, J. Nanosci. Nanotechnol. **11**, 11147 (2011).

44. A. A. Kaminskii, A. G. Petrosyan, G. A. Denisenko, T. I. Butaeva, V. A. Fedorov, and S. E. Sarkisov, Phys. Status Solidi **71**, 291 (1982).

45. M. C. Mesa, P. B. Oliete, R. I. Merino, and V. M. Orera, J. Eur. Ceram. Soc. **33**, 2587 (2013).

46. G. Chai, G. Dong, J. Qiu, Q. Zhang, and Z. Yang, J. Phys. Chem. C **116**, 19941 (2012).

47. N. R. Aghamalyan, R. K. Hovsepyan, E. A. Kafadaryan, R. B. Kostanyan, S. I. Petrosyan, G. H. Shirinyan, G. R. Badalyan, D. G. Zargaryan, A. K. Abduev, and A. S. Asvarov, J. Contemp. Phys. **44**, 291 (2009).

48. G. Wang, O. Marty, C. Garapon, A. Pillonnet, and W. Zhang, Appl. Phys. A Mater. Sci. Process. **79**, pages 1599 (2004).

49. N. Abdellaoui, A. Pereira, T. Kandri, E. Drouard, M. Novotny, B. Moine, and A.

Pillonnet, J. Mater. Chem. C **4**, 9212 (2016).

50. S. Ponmudi, R. Sivakumar, C. Sanjeeviraja, and C. Gopalakrishnan, J. Mater. Sci. Mater. Electron. **30**, 18315 (2019).

51. S. Ponmudi, R. Sivakumar, C. Sanjeeviraja, and C. Gopalakrishnan, J. Mater. Sci. Mater. Electron. **30**, 18315 (2019).

52. R. Eason, Pulsed Laser Depos. Thin Film. **1**, 3 (2006).

53. S. Abubakar, S. Kaya, A. Aktag, and E. Yilmaz, J. Mater. Sci. Mater. Electron. **28**, 13920 (2017).

54. J. Shi, Y. Chen, T. Liu, and H. Liang, J. Dispers. Sci. Technol. **41**, 1471 (2020).